https://doi.org/10.5194/egusphere-2024-3373
Preprint. Discussion started: 13 November 2024

Operational hydrodynamic service as a tool for coastal flood assessment

Xavier Sánchez-Artús[1], Vicente Gracia[1], Manuel Espino[1], Manel Grifoll[1], Gonzalo Simarro[2], Jorge Guillén[2], Marta González[3], and Agustín Sanchez-Arcilla[1]

[1]Universitat Politècnica de Catalunya - BarcelonaTech (UPC), Laboratori d'Enginyeria Marítima (LIM), C/Jordi Girona, 31, 08034, Barcelona, Spain
[2]Institute of Marine Sciences (CSIC), Passeig Marítim de la Barceloneta 37-49, Barcelona, 08003, Spain
[3]Institut Cartogràfic i Geològic de Catalunya (ICGC), Barcelona, Spain

Correspondence: Xavier Sánchez-Artús (xavier.sanchez.artus@upc.edu)

Abstract. A comprehensive, high-resolution hydrodynamic operational service using XBeach model is presented and tested for three urban beaches in Barcelona, NW Mediterranean Sea. The operational architecture is based on Python scripts combined with task automation tools, ensuring a user-friendly system implemented on a standard desktop computer. Hydrodynamic validation of the model is carried out using data gathered during a field campaign in 2022, when a high-intensity storm occurred, resulting in a root mean square error of around 0.4 m and a skill score assessment index of 0.82. Flooding predictions were validated using videometry systems, yielding satisfactory Euclidean distances less than 5 m for storms close to the topobathymetry collection. For storms occurring years earlier, the distances ranged between 7-15 m, underscoring the need for regular topobathymetry updates to maintain forecasting accuracy. The operational system is designed to provide early-warning coastal flooding at three-days horizon. The service provides a warning system with a specific categorisation of the event, enabling the end-users to prepare for a possible flooding. The outcome assists in decision-making of such events by utilizing the operational system. The presented methodology is easily adaptable and replicable to meet user requirements or to be applied in other areas of interest.

1 Introduction

Currently, nearly 600 million people reside in low-lying coastal areas, defined as zones less than 10 metres above mean water level (McGranahan et al., 2007; Idier et al., 2021). These zones are highly susceptible to flooding during storms due to their low elevation (Romero-Martín et al., 2024). Climate change exacerbates this threat by causing sea level to rise, which is expected to increase the frequency and severity of flooding if no additional measures are taken (Cid et al., 2016; IPCC, 2022). Jongman (2018) talks about the necessity to cope with these challenges by implementing diverse solutions such as flood protection measures, risk prevention plans, nature-based solutions approaches, and early warning systems (EWS). Thus, continuous monitoring and protection are required actions to increase the resilience of such areas (Baschek et al., 2017). In addition to these problems, the rapid urbanization in recent decades and the lack of adequate coastal protection infrastructures have increased the impacts of flooding events (Chondros et al., 2021). Hence, stakeholders must have decision-making tools

https://doi.org/10.5194/egusphere-2024-3373
Preprint. Discussion started: 13 November 2024

to mitigate current impacts and prepare the coasts for the future. For the short-term actions, EWS are vital for safeguarding coastal areas by providing enough time to act and minimize the damages before they occur while for long-term, understanding potential impacts under various scenarios is crucial for risk reduction planning.

To efficiently implement these EWS, an operational architecture is necessary to automate all modules and facilitate communication with users, primarily stakeholders, via e-mail, alerts or applications. These channels enable them to make sound decisions before the events occur. To monitor and forecast coastal areas accurately, it is crucial to use different levels of information, from the open sea related to the beach processes among others. Specifically, operational oceanography involves systematic measurement and modeling of seas, oceans, and atmosphere, with rapid data interpretation and dissemination to meet societal and scientific needs (Capet et al., 2020; Schiller et al., 2018). Ocean forecasting, a subset of operational oceanography, uses data and numerical models to predict conditions days in advance (Pérez Gómez et al., 2022). Coastal Ocean Forecasting Systems (COFS) enhance this by focusing on local areas, integrating data from various models and observations, and using coastal models to provide advanced information about the areas of interest (Kourafalou et al., 2015). Increasing integration of coastal observing data for model inputs and calibration improves forecast quality, leading to better decision-making and significant economic and social benefits by reducing storm impact consequences (Walstad and McGillicuddy, 2000; De Mey-Frémaux et al., 2019).

The forecast results provided by models at the coastal areas have to be provided to the stakeholders as swiftly as possible, to give them leeway in the action management (She et al., 2016). Fortunately, advances in technology and computing power over the past few decades have significantly improved the quality of these steps (Pinardi and Woods, 2002). Data can now be analyzed faster, and models can produce reliable results quicker. Moreover, databases have become more accessible, offering high-quality hindcast and forecast data daily. This availability allows for the creation of local systems based on these datasets, focusing only on specific local areas. Modern operational services to forecast coastal areas hazards no longer rely on a single model or a few variables (Mateus et al., 2012); they utilize a combination of data from specialized models to address different issues, such as storm surges, currents, water levels, waves, winds, flooding and erosion. These problems are solved using various meteorologic, hydrodynamic and morphodynamic models, which help reduce computational time and resources (Wilkin et al., 2017; Bogden et al., 2006). This approach also facilitates data collection from servers and the integration of models into a coherent system. Despite these advancements, EWS that forecast coastal flooding still face challenges, such as computational time and the correct calculation of physical hydrodynamic and morphodynamic processes, as noted by Basher (2006). To address them, common solutions include utilizing high-performance computing (HPC) environments, simplifying and reducing the resolution of the model grids, pre-calculating flooding scenarios, and depending on expert judgment instead of strict metrics.

The proposed operational service in this work, created to forecast flooding impacts, tries to solve the previously mentioned challenges using a solution that does not require a complex HPC environment. EWS most important feature is rapidness in obtaining practical results, so the whole strategy must be built around the ability to provide hazard alerts in advance (Quansah et al., 2010; Kelman and Glantz, 2014). Computational and hardware limitations force institutions to develop pre-operational chains that do not become fully operational and only prove effectiveness for specific cases. The developed strategy in this manuscript does not compromise the resolution of the model, as it utilizes hydrodynamic information previously computed

https://doi.org/10.5194/egusphere-2024-3373
Preprint. Discussion started: 13 November 2024

by other models. This data is automatically collected from servers and employed to focus the study on a local area using a coastal hydromorphodynamic model. This methodology provides end-users, typically stakeholders, with forecasting outcomes and relevant information about the study area, including warning alerts to help them with the decision-making about potential hazards.

Then, the objective of this study is to present the architecture of a high-resolution operational service designed to estimate coastal flooding and provide timely results, enabling stakeholders to take action, all while being implementable on a standard desktop computer. To analyze and validate the effectiveness of this system, we have applied it to three urban beaches in Barcelona (NW Mediterranean Sea). These beaches were chosen due to the availability of hydro-topographic data and a videometry system, which facilitated the validation of the operational service.

The manuscript is structured as follows: Section 2 provides the materials and methods including the description of the studied area used for developing the operational tool, an explanation of the system architecture, jointly with the strategy followed to calibrate and validate the models using a field campaign and cameras. Section 3 shows the results of the calibration/validation exercises in terms of hydrodynamics and flooding. Section 4 establishes a discussion of the main characteristics of the system compared with other approaches, the limitation of the strategy itself and model capability; and the possibilities of tuning and improvements of the strategy. Finally, Section 5 summarizes the conclusions of the study.

2 Materials and Methods

2.1 Study area

This study focuses on three urban sandy beaches that are fully integrated into the city of Barcelona, northeastern coast of Spain (NW Mediterranean). From South to North, they are named as Sant Sebastià, Sant Miquel and Barceloneta (Figure 1). The area has a total length of approximately 1.5 km and mean width of 45 m, being the median grain size of about 0.88 mm (CIIRC, 2010). The beaches are among the most visited in the region. The coast, oriented at 20° relative to the north, is fully exposed to storms. The highest intensity events, mainly occurring from October to April, are from the East and North-East directions and can cause severe damage to the existing infrastructures (Ribas et al., 2010).

The impact of storms forces the administration to regularly intervene in the emerged part of the beaches by adding or redistributing the sediment (Turki et al., 2013). Even in a microtidal environment, with a tidal range of approximately 0.25 m (Grifoll et al., 2012), variations in mean sea level can reach up to 0.9 m during storms due to the contribution of strong winds caused by low atmospheric pressure fronts, potentially leading to flooding. At present, the coast is heavily intervened with a small revetment at Sant Sebastià beach, a T-shape groin that separates Sant Miquel and Barceloneta and a double groin at the North of Barceloneta beach (Figure 1). Sant Miquel and Sant Sebastià can be considered as a single unit and they will be referred in this study as SMSS. The backshore is bordered by a seafront promenade that reaches a height of +7.5 m at Barceloneta beach, gradually decreasing towards the south until it reaches +3.5 m. The boardwalk provides access to the coast, as well as numerous establishments, including restaurants and a hotel.

https://doi.org/10.5194/egusphere-2024-3373
Preprint. Discussion started: 13 November 2024

Figure 1. Location map of the study area. a) NW Mediterranean Sea. Blue rectangle marks Barcelona. b) Close-up of southern region of Barcelona beaches. Stars (M1 and M2) show the location of the field campaign deployments. Gray rectangle represents the extent of the computational domain. c) and d) show photographs taken during Celia storm within the study area, at the locations marked by the camera symbols on the general map. These images illustrate the impacts caused by the storm event. Ortophoto obtained from the ICGC WMS.

2.2 Operational architecture

The structure of the developed framework is shown in Figure 2. The chain is controlled with task automation tools, in this case the Task Scheduler application for Windows OS. A similar approach for Linux and MacOS could be implemented with equivalent settings through "at" package commands or Automator and iCalendar respectively. Triggers are arbitrarily selected and subject to changes based on demands. In our application, the chain starts at 02:00h local time and shares the result of the

https://doi.org/10.5194/egusphere-2024-3373
Preprint. Discussion started: 13 November 2024

operational chain at 09:00h through the sending of an e-mail to the competent person. Data request and threshold/flooding analysis are activated through Python scripts linked to the task automation tool.

XBeach (version 1.23) is selected as the core model to simulate the response of the coast. XBeach is a two-dimensional model that encompasses wave propagation, sediment transport and beach morphology changes among other processes (Roelvink et al., 2009, 2010; McCall et al., 2014). The surfbeat mode, which includes infragravity waves, is used in this study to simulate both flooding and coastal changes correctly. Modules for sediment transport and morphology changes are enabled since flooding is heavily influenced by the topobathymetry. The generated mesh, which features a rectangular configuration, has a 5 m resolution on both axes and is oriented to follow beach direction (see Figure 1). Appendix A provides the parameters used in the simulations conducted for this study. Additional parameters, such as the median grain size (0.0008 m) (CIIRC, 2010) and the treatment of the city as a non-erodible layer, are also specified. The grid is referenced to ETRS89 UTM 31N and has been post-processed to improve the water-land interface coupling. A python-based script, employing sub-process commands, activates the trigger for initiating XBeach simulations. The model is configured to run in parallel mode using MPI (Message Passing Interface) settings.

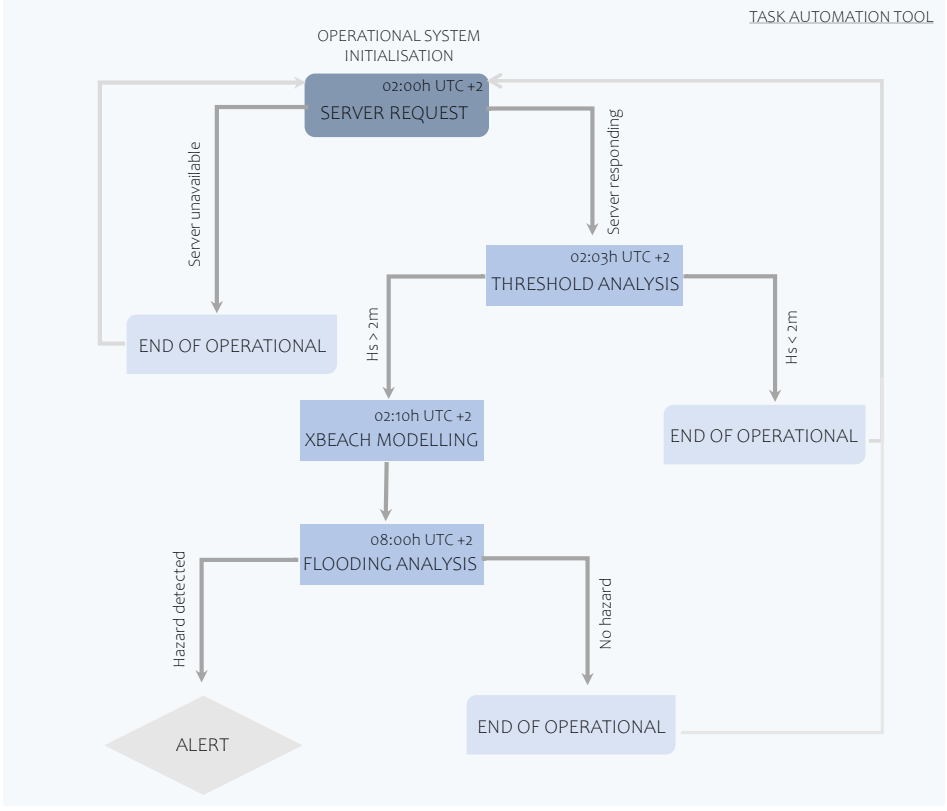

Figure 2. Workflow for the automated operational service. A detailed explanation is provided in Section 2.2.

https://doi.org/10.5194/egusphere-2024-3373
Preprint. Discussion started: 13 November 2024

The chain starts with a hydrodynamic data request to the Copernicus Marine Environment Monitoring Service (CMEMS). It is a European Program for the establishment of a European capacity for Earth Observation, which provides oceanographic products and services for maritime safety, coastal and marine environment, climate and weather forecasting and marine resources users. For the study area, there are two different datasets available: the Atlantic-Iberian Biscay Irish (IBI) database (Aznar et al., 2016) and the Mediterranean Sea database (MEDSEA). For this work, we utilized IBI dataset, although MEDSEA could also be used as a primary input according to the proposed approach. IBI has been used as a boundary condition to build operational downstream services through high-resolution hydrodynamic models (e.g. Sotillo et al. (2020)), offering a daily updated high-resolution ocean analysis and forecast product. Hourly data for significant wave height, peak period, mean direction and water level is requested from the closest CMEMS point to the XBeach computational grid (hereinafter referred to as R1). The information is gathered in the early morning for that same day and the subsequent two, obtaining a three-days forecasting. In the event of server or computer failure during data collection, the operational chain is ended until it can be restarted the following day. However, it can be manually reactivated the same day if necessary.

The next step involves activating XBeach only if a significant wave height exceeding the 2-metre threshold is detected in the forecasted time series from CMEMS. This threshold is commonly used to indicate storm conditions along the Catalan coast (Bosom and Jiménez, 2011). If no such value is observed, the XBeach module is not triggered, and the operational service ends, as it is assumed that no hazards will be identified during the chain. The XBeach results, which take three hours to process on a standard desktop computer, in this study Intel Core i7-10700 with 16 GB RAM, are automatically analyzed to assess the extent of inundation using Equation 1. This equation considers the total number of cells between the coastline and the promenade and compares it to the number of cells that are flooded during the event, yielding the percentage of the flooded beach. To determine the number of flooded cells, an output variable called *wetz* is used.

$$\% \text{ flooded area} = \frac{\text{Number of flooded cells}}{\text{Number of total cells}} \times 100 \tag{1}$$

These percentages are used to establish a color-coded alert level system, helping end-users assess the potential magnitude of the impacts. The alert levels are categorized as follows: green for no alert when 0-25 % of the area is flooded, yellow for moderate alert with 25-50 %, orange for high alert with 50-75 %, and red for extremely high alert with 75-100 %. Additionally, if the forecasted wave height detected is always less than 2 metres, the event is also classified as no alert. Figure 3 illustrates examples of images ranging from no alert to maximum alert, and demonstrates how color scales are used to classify the flood hazard.

Once the analysis of XBeach results is completed, an e-mail is automatically sent to the selected recipients, which can be stakeholders, government authorities or those responsible for the studied area. The user receives each day a status of the study

https://doi.org/10.5194/egusphere-2024-3373
Preprint. Discussion started: 13 November 2024

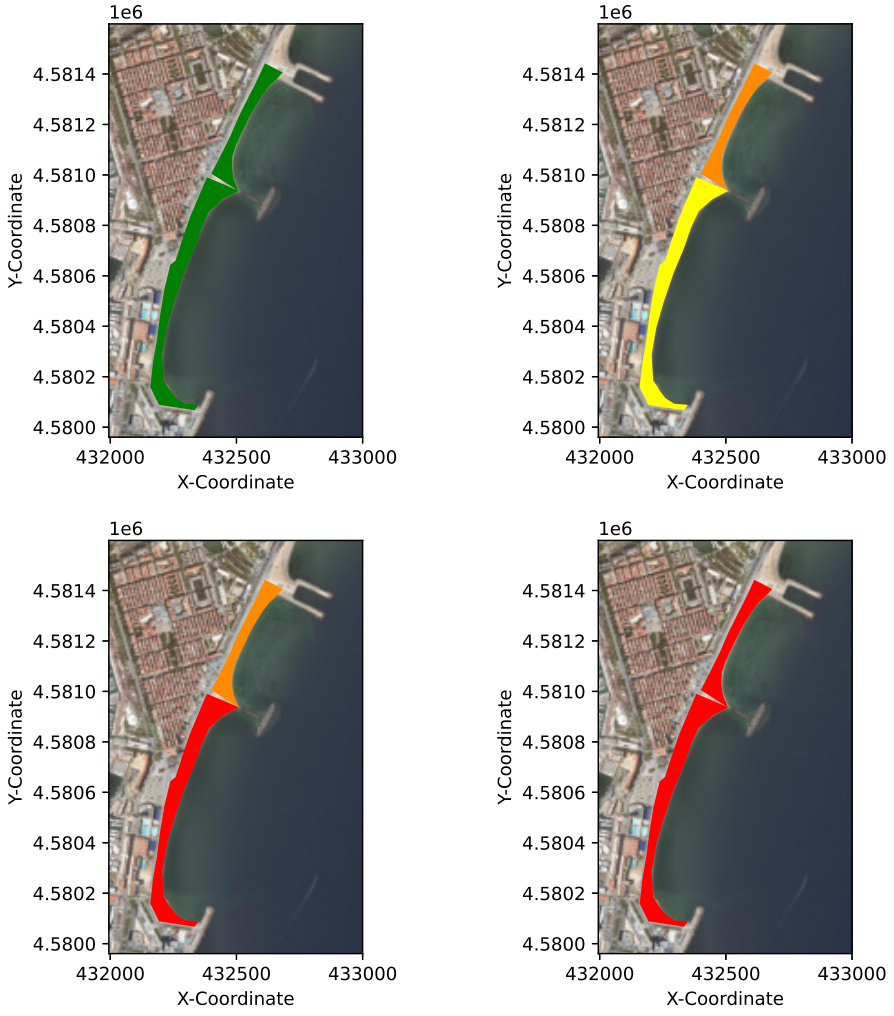

Figure 3. Examples for different alert levels obtained within the e-mail. Green means no alert, yellow moderate alert, orange high alert and red extremely high alert. From least to most impact: top left, top right, bottom left, and bottom right. Ortophoto obtained from the ICGC WMS.

area based on the described alert system, with the corresponding image as in Figure 3. Within the e-mail, a graphical view of the flooded line for the forecast is also attached, in order to ease the comprehension of the magnitude for the possible impact (Figure 4). We chose to prioritize this output type over numerical information because users will find it easier to understand than statistical analysis of the event. Even so, numerical aspects of the impact could be easily included in the e-mail.

The explained workflow corresponds to the demonstration built to show the capacity of the operational service but the developed strategy is fully adaptable and modular. The starting times, the total simulated days, the thresholds and analysis to determine if the alerts trigger, and the core of the sent e-mail, among all the other parts can be totally changed and more

https://doi.org/10.5194/egusphere-2024-3373
Preprint. Discussion started: 13 November 2024

Figure 4. Example of figure received within the e-mail showing the magnitude of flooding, in this case for a high-intensity event. The red line shows the expected flooding line from the forecast. Ortophoto obtained from the ICGC WMS.

modules can be incorporated into the system. Figure 5 shows a complete synthesis of the operational chain, including inputs and the forecasting strategy for the current version.

2.3 Validation strategy

The modelling part of the operational chain has to be validated with test cases beforehand to confirm the results produced by XBeach accurately reproduce the real behavior of the beaches. XBeach model was originally designed for use in sandy beaches, as in the case study, and several papers have demonstrated the model's effective performance in these regions (Sánchez-Artús et al., 2023, 2024; Zhou et al., 2023; Roelvink et al., 2009; Carrion-Bertran et al., 2024) but a proper validation in each study area is needed to ensure the quality of the forecast. In this paper, we explore the validation for two different results.

https://doi.org/10.5194/egusphere-2024-3373
Preprint. Discussion started: 13 November 2024

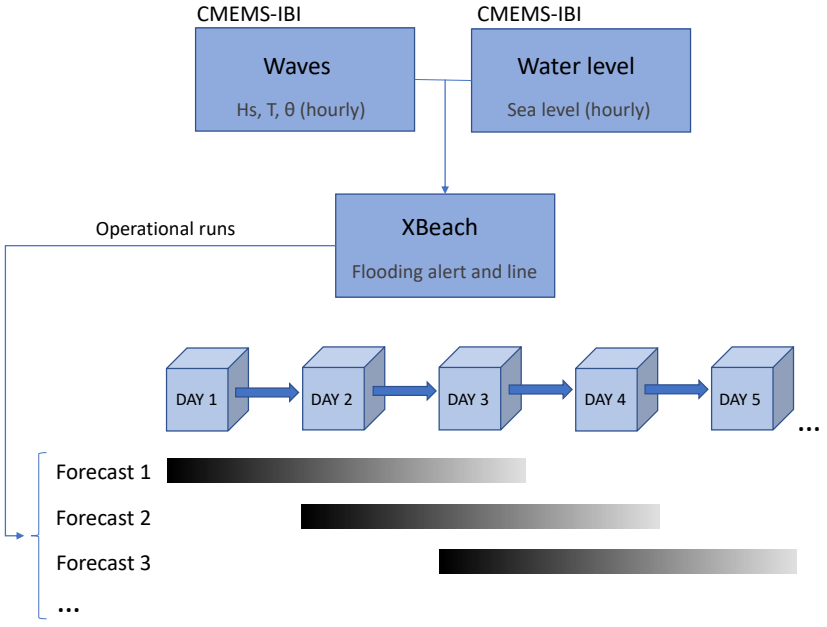

Figure 5. Synthesis of the operational chain. Boxes refers to days of forecast. Horizontal bars define the three-days forecasting simulations through XBeach model using CMEMS-IBI inputs. Gray scale shows qualitative approximation of the accuracy prediction, with black showing higher confidence and light gray lower confidence.

First, the correct representation of the hydrodynamics based on wave height was verified using data from a field campaign conducted from 9th March to 27th April, 2022, as part of the MARLIT project (MARLIT, 2021). Typically, the hydrodynamic component of the model is not re-validated since the model has been widely used and studied, demonstrating that it performs correctly. Still, it is known to slightly underestimate the wave height (De Beer et al., 2021; Oliveira et al., 2020; Buckley et al., 2014). In the campaign, two instrumented benthic tripods, each fixed to a concrete slab, were deployed at 8 m and 13.4 m depth and will be referred hereinafter as M1 and M2 respectively. M1 was located at coordinates 41º22.454'N 2º11.602'E whereas M2 was deployed at 41º22.472'N 2º11.712'E. Wave height, period and direction were hourly acquired by means of two acoustic current profiler (ADCP). M1 mounted a Nortek Aquadopp 2MHz placed at 0.8 m above the bottom, whereas M2 installed a Nortek AWAC 1MHz ADCP ® at 1 m above the bottom at M2. A major storm, named as Celia, was recorded during the campaign (Figure 6). This extreme event exhibited an almost constant wave direction of about 120º at both deployments, being the significant wave height (H_s) at the peak of about 4 m with an associated peak period (T_p) of 10 s. The 15-day storm caused substantial coastal flooding on the beaches, affecting the existing infrastructure (Figure 1). Additionally, two more storms from the East and East-Northeast were recorded at the end of the campaign. Figure 6 shows the wave conditions observed throughout the entire period. In addition, two topo-bathymetric surveys were conducted: the first on 4th March, just before the start of the hydrodynamic measurements, and the second on 24th April, at the end of the campaign. A small vessel

https://doi.org/10.5194/egusphere-2024-3373
Preprint. Discussion started: 13 November 2024

equipped with a multi-beam echo sounder was used for the bathymetry providing data with a horizontal resolution of 1 m. The emerged part was surveyed using an electronic total station by taking measurements along transects perpendicular to the beach and spaced approximately every 10 m. After field collection, data was transferred into a GIS to generate a high-resolution Digital Terrain Model (DTM), which, after post-processing, was converted into the mesh described in Section 2.2.

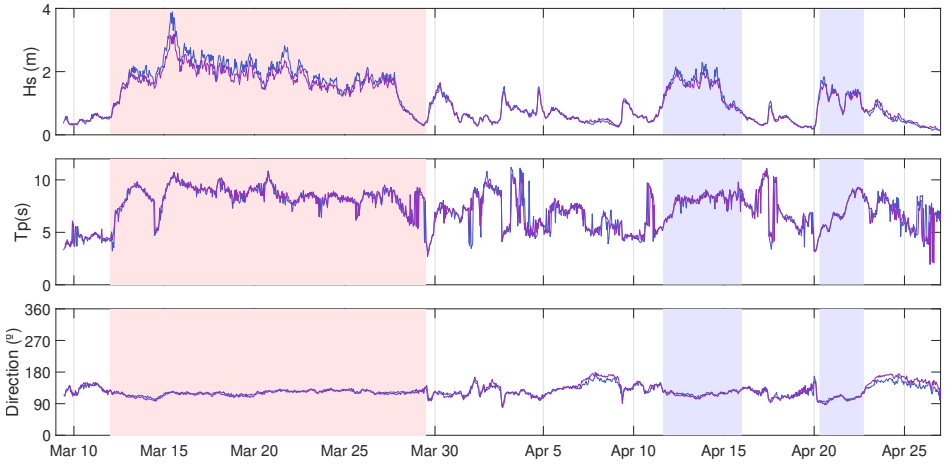

Figure 6. Hydrodynamic analysis of the campaign. Blue line corresponds to M1 and purple line to M2. Red rectangle shows the period when Celia storm hit the coast. Blue rectangles show the two minor storms that occurred during the campaign period.

Then, as the main focus of the operational alert, the model's flooding output was compared with videometry technology. Cameras have the advantage over satellite data in that, if the optical sensor is not heavily covered by rain, it is possible to define the flooding lines in storm conditions. Meanwhile, in the satellite data, clouds typically appear during these periods, making it impossible to detect them. Besides, cameras are able to provide a higher frequency of images for the study area, which improves monitoring. Therefore, for calm periods both are good, but for validation of high-intensity events, which is the main aim of the manuscript, data from cameras work better.

Images of one of the cameras from the Argus-like station in Barcelona city are considered in this work (Figure 7, coo.icm.csic.es) for the validation. This station, placed 142 m above the mean sea level, overviews Barcelona beaches since 2001. The original set of five cameras (Ojeda and Guillén, 2008) was replaced in 2015 by a set of six cameras of higher resolution. The camera over-viewing the beaches of interest in this work (SMSS and Barceloneta, Figure 7) has a resolution of 2452 $\times$ 2056 pixels^2 and provides snapshots, 10-minute time averaged (*timex*) and variance images hourly. For this work, timex images were used to determine flooding lines. The pixel footprint for the beaches of interest is, in the farthest part of the study area (SMSS), $\sim$ 0.6 m in the cross-shore direction, the one of most interest, and $\sim$ 4.5 m in the alongshore direction. The resolution improves in the Barceloneta beach, closer to the station, up to $\sim$ 0.3 m in the cross-shore direction and $\sim$ 0.6 m in the alongshore direction. The cameras have been hourly calibrated using the automatic calibration methodology presented by Simarro et al. (2021) to avoid detected and significant changes of calibrations within the day (mainly due to the dilatation of the building where the

https://doi.org/10.5194/egusphere-2024-3373
Preprint. Discussion started: 13 November 2024

cameras are placed) or due to undesired sudden changes. The images are manually digitised using Python scripts to define the flooding lines, with points in pixel coordinates. The calibration of the cameras allows to transform these pixel coordinates of the shoreline to real world coordinates, provided that z is known at the shoreline. For these type of transformations, ULISES codes (Simarro et al., 2017) and relatives (https://github.com/Ulises-ICM-UPC) were used.

Figure 7. Time averaged (*timex*) image corresponding to April 3th, 2022. From top to bottom: SMSS and Barceloneta, which is the study area of the work, and Somorrostro beaches.

For each type of validation, different error metrics were considered based on data characteristics. The hydrodynamic model's performance was calculated through the Root Mean Square Error (RMSE) and the skill score assessment index (SK) (Equations 2 and 3). RMSE is a widely-used and reliable metric for assessing the relationship between two data series, making it an appropriate choice for evaluating these types of results and models (Williams et al., 2017; McCall et al., 2014; Matias et al., 2019) while SK presents the agreement in a range from 0 to 1, being 0 a complete disagreement and 1 a perfect match between model and observations (Willmott, 1981). The analysis considered the Celia storm as it is the main responsible of changes and the objective of the forecast. In the formulas, the predicted value obtained from the model (P_i) is compared with the observed value from the deployment (O_i) for each point i in the time series, with n representing the total number of points. For SK analysis, the mean values for the observations (with the over bar -) are also considered.

$$RMSE = \sqrt{\frac{\sum_{i=1}^{n} (P_i - O_i)^2}{n}} \tag{2}$$

https://doi.org/10.5194/egusphere-2024-3373
Preprint. Discussion started: 13 November 2024

$$SK = 1 - \frac{\sum_{i=1}^{n} (P_i - O_i)^2}{\sum_{i=1}^{n} \left(|P_i - \bar{O}| + |O_i - \bar{O}| \right)^2} \quad (3)$$

To validate flooding, pre-processing was required before comparing the model and camera data for two reasons. First, the camera data covered a larger area than the model data, so the lines were adjusted to have the same starting and ending points. Second, the datasets differed in the number of data points, with one dataset containing fewer samples than the other, making direct comparison challenging. To address this, the number of points defining each line was resized to coincide between datasets, following the recommendations for such cases (Japkowicz et al., 2000). After these steps, and because the flooding lines and points were defined in a 2D spatial field, the Euclidean distance was used to analyse the differences between both datasets. As described in Equation 4, the distance (d(p, q)) quantifies the difference between each point on the observed flooding line from the camera (p) and the corresponding point from the model output line (q). In this equation, p_1 and q_1 represent the x-coordinates, while p_2 and q_2 represent the y-coordinates of the points (p) and (q), respectively. Finally, the mean of the distances between corresponding points was computed to determine the average distance between the flooding observed by the camera and the model output, in metres.

$$d(p, q) = \sqrt{(p_1 - q_1)^2 + (p_2 - q_2)^2} \quad (4)$$

In addition to the Celia storm, which was used for both hydrodynamic and flooding validation, other storms were tested to enhance confidence in the model's flood results. Emphasizing their intensity, several storms documented by newspapers and the flooding magnitude captured by the camera were examined. Scenarios with significant flooding were selected as validation cases, ensuring that various years were accurately represented and avoiding the selection of storms from only one or two years. Also, to enrich the study, two different calm periods were tested: one close to the time of the topobathymetry realisation and another from a year later, to observe changes in the coastline position. Table 1 provides a summary of the characteristics for the chosen storms and the calm periods.

Table 1. Characteristics for the storm and calm events studied at the CMEMS reference point (R1).

Storm event	**Date**	**Maximum H_s (m)**	**Maximum T_p(s)**	**Maximum WL (m)**
OCT19	October 2019	2.2	9.1	0.89
DEC19	December 2019	3.7	10.5	0.93
Gloria	January 2020	4.7	11.9	0.69
Celia	March 2022	4.0	10.0	0.50
Isaak	February 2023	4.0	10.0	0.55
Calm periods				
Calm 1	March 2022	0.19	7.9	0.75
Calm 2	June 2023	0.5	5.6	0.60

https://doi.org/10.5194/egusphere-2024-3373
Preprint. Discussion started: 13 November 2024

3 Results

3.1 Hydrodynamic validation

Figure 8 illustrates the comparison between the model results and observed values from both M1 and M2 during storm Celia. At M2, the model shows a closer match with the observed data at the storm's peak, whereas for M1 position, it slightly underestimates the wave height. Despite this, the discrepancies for both deployments are mainly observed during the setup and end phases of the storm, with the peak, typically associated with maximum flooding, being the most accurately represented. Quantitatively, the analysis obtained an RMSE of 0.33 m at M2, while at M1, it increased to an RMSE of 0.49 m for the period corresponding to the storm passing. For SK analysis, M2 achieved a value of 0.86 out of 1, and for M1 it decreased until 0.80. However, both values still represent a great agreement between the model and the observed data (see Figure 8).

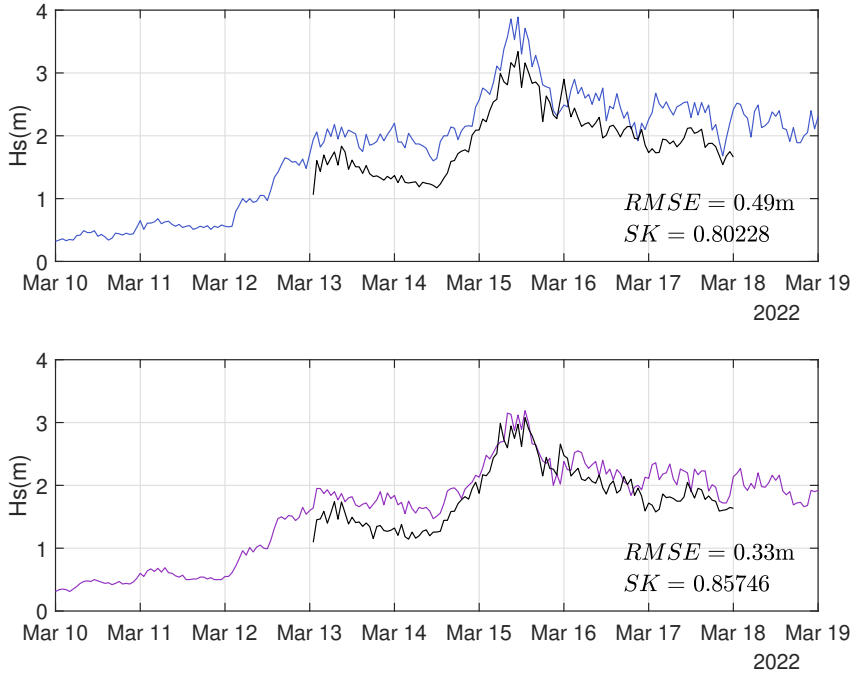

Figure 8. Hydrodynamic response validation of the model. Top panel and the light blue line corresponds to M1 while bottom panel and purple line to M2. Black lines show the model output for each point.

3.2 Flooding validation and sensitivity analysis

Figure 9 illustrates the conditions for SMSS and Barceloneta beaches during the studied storm events. Figure 10 presents results for both SMSS and Barceloneta beaches under the calm condition scenarios. Additionally, Table 2 summarizes the Euclidean distances obtained for all the studied cases.

https://doi.org/10.5194/egusphere-2024-3373
Preprint. Discussion started: 13 November 2024

In the context of the Celia storm, which is the storm most closely aligned with topobathymetric data and when the hydrodynamic validation during field campaigns was done, the comparison depicted in Figure 9 reveals a strong correlation between the model and the camera across SMSS beaches, as well as with Barceloneta beach. Supporting this observation, Table 2 provides quantitative evidence with obtained values from the Euclidean distance analysis of 2.7 m for SMSS beaches and 2.9 m for Barceloneta. Given the 5x5 m mesh resolution, this error is considered sub-pixel, suggesting that further theoretical improvements may not lead to real enhancement of the accuracy.

For the other studied storms similar patterns emerge, as depicted in Figure 9 for SMSS beaches. The qualitative alignment, relevant for decision-making in the operational chain as visual component, demonstrates a consistent match between both datasets. Notably, discrepancies tend to appear at the extremities of the beaches, while the central areas exhibit the highest coherence between videometry data and the model. Specifically, the biggest differences are observed for the Gloria storm. The causes were the difficulty of simulating this long and extremely high-intensity event along with the challenge of precisely defining the flooding line from the cameras due to heavy rain obscuring the lens and resulting in poor visibility. Two different time frames were simulated in an attempt to achieve more stable results, but the mentioned issues persisted in both study periods. The other storms exhibit a strong correlation between the camera and model results, with smaller distance discrepancies for storms closer to the topobathymetry gathering. As shown in Table 2, Celia storm had the best approximation, followed by Isaak, both achieving subpixel accuracy. Conversely, the accuracy decreased for storms that were farther away, with OCT19 storm of 2019 showing the highest euclidean distance value, of 12 m, excluding Gloria storm.

For Barceloneta beach, as it can also be seen in Figure 9, the behaviour is similar as for SMSS. In this case, discrepancies generally does not exceed twice the mesh resolution (i.e. 10 m), except in the case of the Gloria storm. Comparing with SMSS, Barceloneta better catches the flooding of the storm for all the studied scenarios except for Celia, where as explained before, subpixel accuracy does not determine a difference between these values. Besides, the same pattern is observed where the model seems to underestimate the southern part of the beach flooding while overestimating the flooding in the northern parts. For the central parts, the correlation is the highest, as it can be observed in Figure 9.

Calm conditions, as shown in Figure 10 for both studied cases, show a good visual correlation. The greatest differences were observed for Barceloneta beach during the calm conditions of June 2023, followed by SMSS for the same period. In contrast, the accuracy obtained for the calm scenario closer to the topobathymetry gathering was subpixel, following the same pattern as for storm conditions as it can be seen in Table 2. In this case, since the waves do not greatly affect the dynamics and the flooding is minimal, the differences between the model and the camera are more homogeneous for Barceloneta beach, with the model consistently overestimating the coastline alongshore. For SMSS, although the overall correlation is higher, the model seems to slightly overestimate the camera at the beach extremities, while the center shows the best match.

3.3 Operational analysis

The metric used to characterize storms within the operational service, as described in Section 2.2, was applied to various storms during the validation process to evaluate the effectiveness of the alert system. Table 3 presents the alert levels obtained for different storms at each beach. Gloria storm is the only one reaching a red alert level, indicating an extremely high alert,

https://doi.org/10.5194/egusphere-2024-3373
Preprint. Discussion started: 13 November 2024

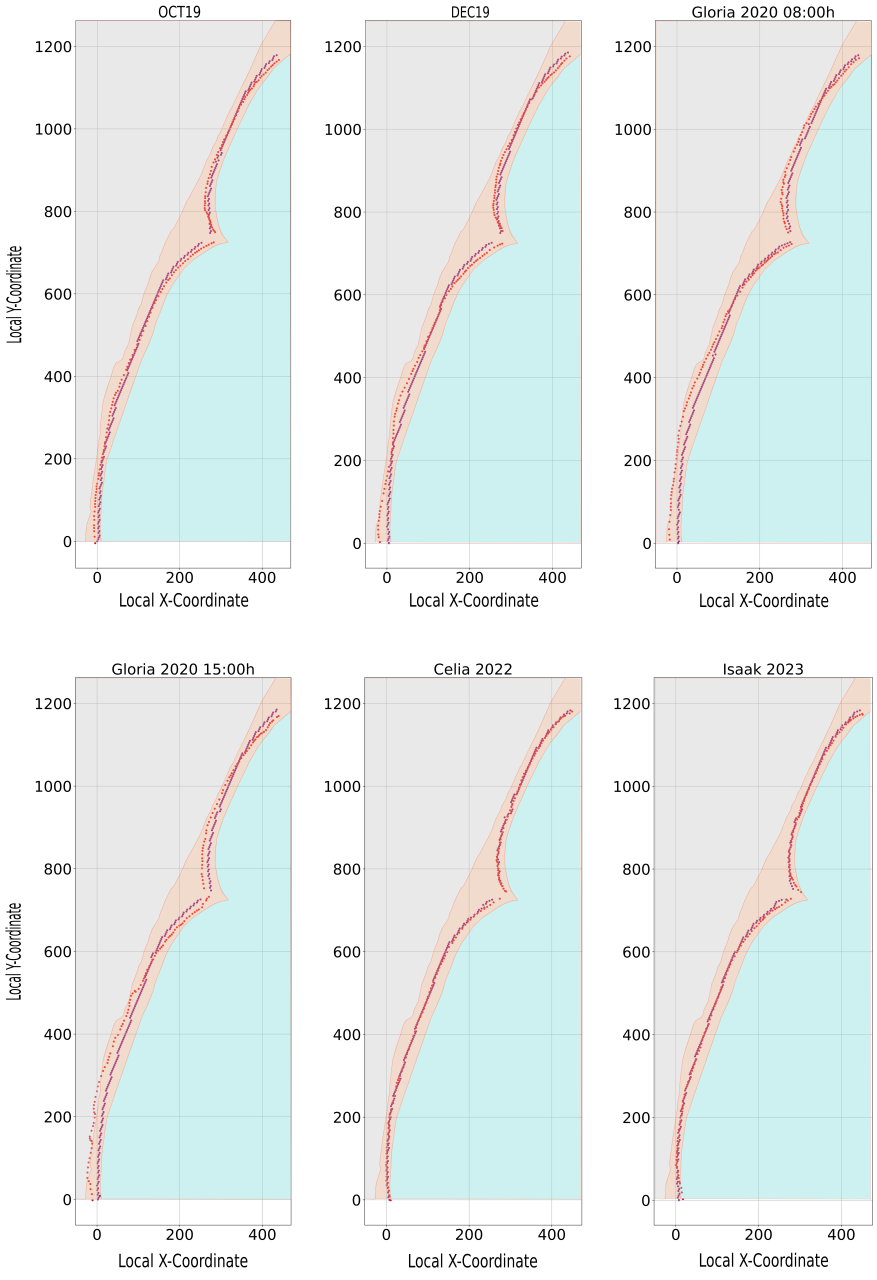

Figure 9. Comparison of the flooding for selected storm events. In purple, model results; in red, videometry. Light brown polygon indicates the extent of the beaches, blue represents water, and gray denotes the promenade and the city. Local axes are used, with distances measured in metres.

https://doi.org/10.5194/egusphere-2024-3373
Preprint. Discussion started: 13 November 2024

Table 2. Euclidean distance, in metres, for each of the storm and calm conditions, separated for both studied areas.

Storm	SMSS	Barceloneta
OCT19	7.7	6.5
DEC19	12.0	7.7
Gloria 2020 08:00h	17.5	10.7
Gloria 2020 15:00h	16.8	13.0
Celia 2022	2.7	2.9
Isaak February 2023	3.9	3.8
Calm March 2022	4.4	4.8
Calm June 2023	6.5	9.5

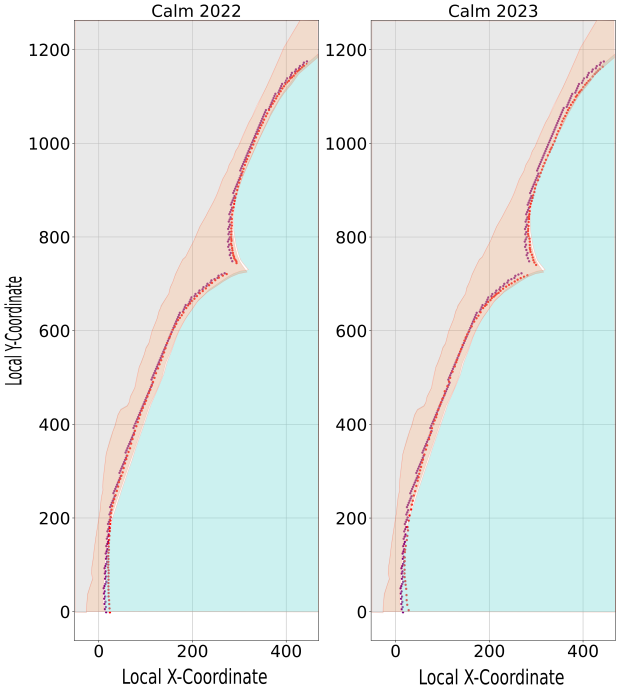

Figure 10. Comparison of the flooding for selected calm conditions. In purple, model results; in red, videometry. Light brown polygon indicates the extent of the beaches, blue represents water, and gray denotes the promenade and the city. Local axes are used, with distances measured in metres.

with flooding areas of 81.3 % at SMSS beaches and 83.2 % at Barceloneta. OCT19 and DEC19 storms triggered orange alerts, classified as high alert, for both SMSS and Barceloneta beaches. The flooding areas for OCT19 were 53.6 % and 51.3 %, while for the DEC19 storm, they were 60 % and 68.9 %, respectively. Celia and Isaak storms resulted in an orange alert for

https://doi.org/10.5194/egusphere-2024-3373
Preprint. Discussion started: 13 November 2024

SMSS beach, with flooding areas of 51 % and 60 %, but only a yellow alert, indicating a moderate level, for Barceloneta. The flooding areas for Celia and Isaak at Barceloneta were 33.9 % and 45.8 %, respectively. Finally, during the calm periods, although the operational chain would have stopped before XBeach activation due to low wave height, the hypothetical flooding areas obtained would have been less than 0.1 % in both events.

Table 3. Flooding percentages for studied storms and calm periods at SMSS and Barceloneta beaches.

Storm	SMSS	Barceloneta
OCT19	51.3 %	53.4 %
DEC19	68.9 %	60.0 %
Gloria 2020	83.2 %	81.3 %
Celia 2022	51 %	33.9 %
Isaak February 2023	60 %	45.8 %
Calm March 2022	<0.1 %	<0.1 %
Calm June 2023	<0.1 %	<0.1 %

4 Discussion

4.1 Modelling uncertainties

XBeach was used to simulate the beaches response within the operational chain. The validation of both hydrodynamics and flooding indicated that the model is an effective forecasting tool for inundation at SMSS and Barceloneta beaches, delivering results in a reasonable computational time. However, during the sensitivity test conducted using the complete set of different storm conditions, some discrepancies were identified between the model results and camera observations, which increased the further the storm date was from the topobathymetry survey conducted on 4th March, 2022. This is likely due to the fact that the topobathymetry is reset to its initial state at the start of each forecast simulation, suggesting that accurate topobathymetry is crucial for the model's performance, corroborating previous findings stating that bathymetry significantly influences XBeach output (Mickey et al., 2020; Schweiger et al., 2020; Matheen et al., 2019, 2021). To maintain an operational chain which remains reliable at long-term, with the methodology described in this manuscript, regular updates of the topobathymetry are necessary to enhance model accuracy. Given the high costs associated with this, a more feasible approach could be to periodically correct the coastline and adjust the shallower zones based on the lines extracted from the cameras, obtain an inferred bathymetry using video imagery (Simarro et al., 2019) or a combination of both strategies. This would help to better align the initial beach states with reality. The critical area appears to be the interface between the water and the coast, corresponding to the coastline, as this is where waves consistently impact (Armenio et al., 2019; Koroglu et al., 2019; Ojeda and Guillén, 2008; Franz et al., 2017). This was also observed in this study: during calm conditions in 2023, the differences were more pronounced compared to those in 2022 (see Figure 10), whereas the differences between Celia and Isaak storms, which had

https://doi.org/10.5194/egusphere-2024-3373
Preprint. Discussion started: 13 November 2024

similar intervals, were less significant. Storms, by surpassing this dynamic coastal interface and reaching more stable areas, reproduced flooding impacts more accurately, resulting in outcomes closer to reality. However, for storms occurring years apart, the discrepancies increase because the overall beach dynamics change, and the starting conditions of the coastline prior to the start of the storm differ more significantly. Despite this, the use of videometry allowed the validation of flooding events, as it makes possible the observation of flooding lines under storm effects, which is very challenging with satellite data due to cloud coverage (Li et al., 2022; Shen et al., 2015; Fernandez-Moran et al., 2021). As stated by Arriaga et al. (2022), camera and video monitoring has become an indispensable tool to understand beach processes, and a lot of system have been developed such as ARGUS (Holman and Stanley, 2007), SIRENA (Nieto et al., 2010), BEACHKEEPER (Brignone et al., 2012), or COSMOS (Taborda and Silva, 2012). Also, other camera-based initiatives have been designed, such as KOSTASystem (Liria et al., 2021), that underscore the need for continuous beach monitoring to enhance current approaches and models; and CoastSnap (Harley and Kinsela, 2022), that leverages citizen science, encouraging people to take photographs from specific locations with their smartphones. This not only involves the community in the study but also increases the amount of data collected, demonstrating among the other initiatives the necessity to use videometry and constant monitoring to improve the modelling field.

The results also indicate that the euclidean distances differences at SMSS beaches are larger than those at Barceloneta (see Table 2). One reason for this could be that during the topobathymetry survey, ongoing works at the groyne located at the south of the SMSS beaches prevented the vessel from conducting bathymetric measurements in the area near to the structure. To address this data gap, interpolation was used, which may have reduced the accuracy. Additionally, the flooding lines for Barceloneta beach were easier to define in the images due to its closer proximity, which benefits from increased pixel resolution as described in Section 2.3. This higher resolution allows for better image calibration, easing the process of defining the flooding lines and improving the precision of the statistical analysis.

Regarding the hydrodynamics, the results indicate an underestimation of wave height in shallow waters. This could happen due to several issues. The input waves from CMEMS are taken from the nearest point to the domain as a single point, which does not precisely correspond with the offshore boundary of the domain. Additionally, the significant resolution difference between CMEMS and the local grid introduces uncertainties, largely due to the absence of a downscaling process (Stanev et al., 2016). A potential solution could be nesting XBeach with a hydrodynamic model like SWAN (Booij et al., 1999) or similar. This model would provide wave data at exact multiple offshore locations within the XBeach computational boundary, capturing variations in wave height and direction more accurately across different points, and it is more computationally efficient in larger areas as it does not require high-resolution bathymetry, thereby incorporating the CMEMS point within the domain. Besides, SWAN could be also used to smooth the transition between input and XBeach and ensure better integration of data. However, this strategy was not implemented in the current study and it is planned to be deeply analysed as future research since incorporating another model introduces its own set of problems and errors, and it would increase computational time, reducing one of the key advantages of the current approach. Additionally, the study area is formed by a group of enclosed beaches separated by a groyne (see Figure 1). This configuration produces complex physics, by altering wave propagation due to this structure, which are more difficult to replicate by the model (Scott et al., 2016). At the deeper validation point, situated outside the beginning of the enclosed area, the wave magnitudes are more accurately reproduced at the peak of the storm, as shown in Figure 8. This

https://doi.org/10.5194/egusphere-2024-3373
Preprint. Discussion started: 13 November 2024

improvement can likely be attributed to the simpler and more stable bathymetry at these depths. Besides, unlike in shallower waters, the groyne's influence on wave dynamics is minimal here and the difference in wave height between the CMEMS point and the deployment point is less pronounced at these greater depths.

Finally, the results from the flooding analysis indicate that the model successfully identifies all the studied storm events and accurately distinguishes periods of calm. The proposed metric classifies each event as hazardous storms, identifying Gloria as the most significant, despite some inaccuracies in validation through videometry. This finding enhances the overall strategy and demonstrates that even though the accuracy concerning flooding lines is reduced over time, the approach remains capable of detecting the storms and provide alerts.

4.2 Operationality

The primary aim of the study was to develop a comprehensive methodology that works on a standard desktop computer, while still providing timely feasible coastal flooding forecasts. The proposed strategy meets these initial requirements while allowing the implementation of new features. For example, scripts to define erosion and sedimentation rates, other statistical analyses, or error variability could be added with minimal impact on computational time, enhancing the strategy's modularity. The current study focused on defining the methodology and developing a beta version, which is presented here but not publicly accessible. Nevertheless, the approach is well-advanced, achieving a Technology Readiness Level (TRL) of 6 out of 9, as classified by NASA and described in detail by Mankins et al. (1995). In this case, the approach was adapted to software solutions by Horizon 2020, with level 6 indicating a "beta version of the software functionalities tested by selected end-users under controlled conditions", which is the current state of the work. Advancing to TRL 8, implying a stable version available for the market, and TRL 9, with the version available with full business plan conditions, is not currently planned as it is not intended to commercialize the product. Instead, the goal is to reach TRL 7, ensuring that the functionalities are widely available to end-users in an open and accessible manner.

The proposed operational approach, illustrated in Figure 5, entails an easy increasing of the number of the forecasted days as user demand. However, this would result in longer simulation times and therefore, the competent person receiving the output later. Additionally, the model's accuracy is reduced with longer simulations due to the accumulation of input and model errors. In the current approach, data is requested at 02:00h UTC +2 and results are e-mailed by 09:00h UTC +2, while the computational time of XBeach model is only around three hours to provide the forecasting. Then, with the current hardware specifications, the forecasted days could still be slightly increased but it was not done as this version was planned as a beta version. For this study, a computer with an i7-10700 and 16GB of RAM was used. Using a more powerful PC would accelerate the whole chain but increasing costs. The strategy is presented across three beaches, covering only a few kilometres. However, it may encounter computational limitations when applied to larger areas, as the operational chain would require significantly more time to produce the forecasting. This approach was specifically designed for local areas, where stakeholders make decisions for smaller, focused regions. If larger areas need to be studied, it would be necessary to distribute the operational service across multiple computers, with each handling a specific area of action.

https://doi.org/10.5194/egusphere-2024-3373
Preprint. Discussion started: 13 November 2024

Table 4 outlines the procedures for various failures in the operational chain. As shown, if the operational forecast is interrupted due to server or connection issues, the system ceases to provide information and automatically restarts the following day. In the case of a model crash, the system follows the same procedure, but if the issue persists, for this problem and connection errors, manual intervention is required. In contrast, if a computer crash occurs, the system must be manually restarted to ensure the forecast is available the next day. However, if a problem is detected, the entire chain of scripts can be manually rerun, thereby preventing a loss of prediction for that day. Finally, if major updates need to be made to the computer, the chain must be paused until they are completed. Conversely, if a new version of the model or programming language is released, the operational chain can continue running with the previous version until the new one is fully implemented.

Table 4. Recover procedures for operational chain problems. * means automatic restart but if the problem persists, manual actions are required.

	Automatic	Manual
Server unavailable	X	
Connection error with server	X*	
XBeach crash	X*	
Computer crash		X

The system has been developed as a beta version to provide advance notice of potential flooding impacts during high-intensity storm conditions, allowing for the implementation of quick defence measures to mitigate associated damages as for example in the promenade, showers or beach bars (Figure 1). The proposed methodology is designed to be easily adaptable for other local areas of similar small scale, provided that initial forcing forecasts are available. Previous EWS like iCoast and Risc-Kit (Van Dongeren et al., 2018) aimed for a similar approach but are not currently operational due to the nature of the project. The goal of the presented strategy is to remain available over time and improve its quality through user feedback. For example, communication with Barcelona's port authorities has highlighted the system's utility for medium storms, where flooding is not extreme, and thus, no damage occurs to infrastructures. In such cases, the system can help to prepare in advance the decision for a beach closing to recreational use with red or yellow flags. Currently, in Catalonia, this task is based solely on meteorological forecasts. The introduction of wave and flooding data will significantly enhance decision-making in these cases.

5 Conclusions

This scientific contribution presents a comprehensive high-resolution operational system for assessing coastal flooding. This system utilizes Python scripts and task automation tools, enabling the optimization of local operational systems to predict flooding hazards during storms accurately. The model has been validated for both hydrodynamics and flooding, demonstrating its feasibility and accuracy using data from a field campaign and videometry. The loss of accuracy observed in the studied storms that took place long after the topobathymetry data was collected, indicates that regularly updating the topobathymetry

https://doi.org/10.5194/egusphere-2024-3373
Preprint. Discussion started: 13 November 2024

is an effective strategy for improving long-term results. A field campaign has been used to successfully validate the hydrodynamics, and cameras have been shown to be valuable tools for studying storm events. The defined alert system based on colors has been used to characterized the validated storms, demonstrating the ability of the service to detect flooding hazards. The system ability to send daily forecast updates via e-mail suggests a communication with users and besides, the modular approach allows the inclusion of simple graphical images to complex statistical analyses and data, easing to meet their requirements. Future research could explore the introduction of hindcast data into the forecasting chain to enhance model accuracy further. Additionally, the use of videometry to infer bathymetry and correct the coastline presents a promising avenue for improving predictive capabilities at long-term and further development could also focus on incorporating additional features, such as identifying predominant areas of erosion or specifying hazards based on vulnerable elements.

Code availability. The code supporting the conclusions of this article will be made available by the authors on request.

Data availability. The raw data supporting the conclusions of this article will be made available by the authors on GitHub after the finalisation of REST-COAST project. Meanwhile, data can be provided by authors on request.

Author contributions. Conceptualization, X.S-A. and V.G., M.G.; methodology, X.S-A., V.G., M.G., G.S and J.G.; software, X.S-A., G.S. and J.G.; validation, X.S-A., G.S. and J.G.; formal analysis, X.S-A., V.G., M.E., M.G. and A.S-A.; investigation, X.S-A., V.G., M.G., M.E., G.S., J.G., M.G.D. and A.S-A. ; resources, V.G., M.E., M.G.D. and A.S-A.; data curation, X.S-A., G.S. and J.G.; writing—original draft preparation, X.S-A., V.G., M.G., G.S., J.G. and M.G.D; writing—review and editing, X.S-A., V.G., M.E., M.G., G.S., J.G., M.G.D. and A.S-A.; visualization, X.S-A.; supervision, V.G., M.E., M.G., M.G.D. and A.S-A.; project administration, V.G., M.E. and A.S-A.; funding acquisition, V.G., M.E. and A.S-A. All authors have read and agreed to the published version of the manuscript.

Funding

This project has received funding from the European Union's Horizon 2020 research and innovation programme under grant agreement No. 101037097 (REST-COAST project).

Competing interests. The authors declare that they have no conflict of interest.

https://doi.org/10.5194/egusphere-2024-3373
Preprint. Discussion started: 13 November 2024

Acknowledgements. With the support from the Secretariat for Universities and Research of the Ministry of Business and Knowledge of the Government of Catalonia and the European Social Fund. This study has been conducted using E.U. Copernicus Marine Service Information; 10.48670/moi-00025, 10.48670/moi-00027.

Appendix A: Numerical Model Configuration

The XBeach initial and boundary conditions, along with the parameters used in the simulation presented in this study, are summarized in Table A1.

Table A1. XBeach boundary conditions and physical parameters. The other parameters are defined as default.

PARAMETER	INPUT
back	abs_2d
front	abs_2d
wbctype	jonstable
wavemodel	surfbeat
lateralwave	wavecrest
bedfriction	manning
waveform	2
form	2
sedtrans	1 (activated)
morphology	1 (activated)
struct	1 (activated)
snells	1 (activated)
dilatancy	1 (activated)
CFL	0.7
morfac	10
dryslp	1.5
wetslp	0.8
hswitch	0.5
facua	0.15
gamma	0.78
gammax	3
facsl	0.15
bedfriccoef	0.0325

https://doi.org/10.5194/egusphere-2024-3373
Preprint. Discussion started: 13 November 2024

References

Armenio, E., De Serio, F., Mossa, M., and Petrillo, A. F.: Coastline evolution based on statistical analysis and modeling, Natural Hazards and Earth System Sciences, 19, 1937–1953, 2019.

Arriaga, J., Medellin, G., Ojeda, E., and Salles, P.: Shoreline Detection Accuracy from Video Monitoring Systems, Journal of Marine Science and Engineering, 10, 95, https://doi.org/10.3390/jmse10010095, 2022.

Aznar, R., Sotillo, M., Cailleau, S., Lorente, P., Levier, B., Amo-Baladrón, A., Reffray, G., and Álvarez-Fanjul, E.: Strengths and weaknesses of the CMEMS forecasted and reanalyzed solutions for the Iberia–Biscay–Ireland (IBI) waters, Journal of Marine Systems, 159, 1–14, https://doi.org/10.1016/j.jmarsys.2016.02.007, 2016.

Baschek, B., Schroeder, F., Brix, H., Riethmüller, R., Badewien, T. H., Breitbach, G., Brügge, B., Colijn, F., Doerffer, R., Eschenbach, C., et al.: The coastal observing system for northern and arctic seas (COSYNA), Ocean science, 13, 379–410, https://doi.org/10.5194/os-13-379-2017, 2017.

Basher, R.: Global early warning systems for natural hazards: systematic and people-centred, Philosophical transactions of the royal society a: mathematical, physical and engineering sciences, 364, 2167–2182, 2006.

Bogden, P., Allen, G., Stone, G., MacLaren, J., Creager, G., Flournoy, L., Zhao, W., Graber, H., Graves, S., Conover, H., et al.: The SURA coastal ocean observing and prediction program (SCOOP) service-oriented architecture, in: OCEANS 2006, pp. 1–6, IEEE, https://doi.org/10.1109/OCEANS.2006.306830, 2006.

Booij, N., Ris, R. C., and Holthuijsen, L. H.: A third-generation wave model for coastal regions: 1. Model description and validation, Journal of geophysical research: Oceans, 104, 7649–7666, https://doi.org/10.1029/98JC02622, 1999.

Bosom, E. and Jiménez, J.: Probabilistic coastal vulnerability assessment to storms at regional scale–application to Catalan beaches (NW Mediterranean), Natural hazards and Earth system sciences, 11, 475–484, https://doi.org/10.5194/nhess-11-475-2011, 2011.

Brignone, M., Schiaffino, C. F., Isla, F. I., and Ferrari, M.: A system for beach video-monitoring: Beachkeeper plus, Computers & geosciences, 49, 53–61, https://doi.org/10.1016/j.cageo.2012.06.008, 2012.

Buckley, M., Lowe, R., and Hansen, J.: Evaluation of nearshore wave models in steep reef environments, Ocean Dynamics, 64, 847–862, https://doi.org/10.1007/s10236-014-0713-x, 2014.

Capet, A., Fernández, V., She, J., Dabrowski, T., Umgiesser, G., Staneva, J., Mészáros, L., Campuzano, F., Ursella, L., Nolan, G., et al.: Operational modeling capacity in European Seas—an EuroGOOS perspective and recommendations for improvement, Frontiers in Marine Science, 7, 129, https://doi.org/10.3389/fmars.2020.00129, 2020.

Carrion-Bertran, N., Falqués, A., Ribas, F., Calvete, D., de Swart, R., Durán, R., Marco-Peretó, C., Marcos, M., Amores, A., Toomey, T., et al.: Role of the forcing sources in morphodynamic modelling of an embayed beach, Earth Surface Dynamics, 12, 819–839, https://doi.org/10.5194/esurf-12-819-2024, 2024.

Chondros, M., Metallinos, A., Papadimitriou, A., Memos, C., and Tsoukala, V.: A coastal flood early-warning system based on offshore sea state forecasts and artificial neural networks, Journal of marine science and engineering, 9, 1272, https://doi.org/10.3390/jmse9111272, 2021.

Cid, A., Menéndez, M., Castanedo, S., Abascal, A. J., Méndez, F. J., and Medina, R.: Long-term changes in the frequency, intensity and duration of extreme storm surge events in southern Europe, Climate Dynamics, 46, 1503–1516, https://doi.org/10.1007/s00382-015-2659-1, 2016.

CIIRC: Estat de la zona costanera a Catalunya, International Centre for Coastal Resources Research, 2010.

https://doi.org/10.5194/egusphere-2024-3373
Preprint. Discussion started: 13 November 2024

De Beer, A., McCall, R., Long, J., Tissier, M., and Reniers, A.: Simulating wave runup on an intermediate–reflective beach using a wave-resolving and a wave-averaged version of XBeach, Coastal Engineering, 163, 103 788, https://doi.org/10.1016/j.coastaleng.2020.103788, 2021.

De Mey-Frémaux, P., Ayoub, N., Barth, A., Brewin, R., Charria, G., Campuzano, F., Ciavatta, S., Cirano, M., Edwards, C. A., Federico, I., et al.: Model-observations synergy in the coastal ocean, Frontiers in Marine Science, 6, 436, https://doi.org/10.3389/fmars.2019.00436, 2019.

Fernandez-Moran, R., Gómez-Chova, L., Alonso, L., Mateo-García, G., and López-Puigdollers, D.: Towards a novel approach for Sentinel-3 synergistic OLCI/SLSTR cloud and cloud shadow detection based on stereo cloud-top height estimation, ISPRS Journal of Photogrammetry and Remote Sensing, 181, 238–253, 2021.

Franz, G., Delpey, M. T., Brito, D., Pinto, L., Leitão, P., and Neves, R.: Modelling of sediment transport and morphological evolution under the combined action of waves and currents, Ocean Science, 13, 673–690, https://doi.org/10.5194/os-13-673-2017, 2017.

Grifoll, M., Aretxabaleta, A. L., Espino, M., and Warner, J. C.: Along-shelf current variability on the Catalan inner-shelf (NW Mediterranean), Journal of Geophysical Research: Oceans, 117, https://doi.org/10.1029/2012JC008182, 2012.

Harley, M. D. and Kinsela, M. A.: CoastSnap: A global citizen science program to monitor changing coastlines, Continental Shelf Research, 245, 104 796, https://doi.org/10.1016/j.csr.2022.104796, 2022.

Holman, R. A. and Stanley, J.: The history and technical capabilities of Argus, Coastal engineering, 54, 477–491, https://doi.org/10.1016/j.coastaleng.2007.01.003, 2007.

Idier, D., Aurouet, A., Bachoc, F., Bailly, A., Betancourt, J., Gamboa, F., Klein, T., López-Lopera, A. F., Pedreros, R., Rohmer, J., et al.: A user-oriented local coastal flooding early warning system using metamodelling techniques, Journal of Marine Science and Engineering, 9, 1191, https://doi.org/10.3390/jmse9111191, 2021.

IPCC: Climate Change 2022: Impacts, Adaptation and Vulnerability, Summary for Policymakers, Cambridge University Press, Cambridge, UK and New York, USA, ISBN 9781009325844, 2022.

Japkowicz, N. et al.: Learning from imbalanced data sets: a comparison of various strategies, in: AAAI workshop on learning from imbalanced data sets, vol. 68, pp. 10–15, AAAI Press, Menlo Park, 2000.

Jongman, B.: Effective adaptation to rising flood risk, Nature communications, 9, 1986, 2018.

Kelman, I. and Glantz, M. H.: Early warning systems defined, Reducing disaster: Early warning systems for climate change, pp. 89–108, https://doi.org/10.1007/978-94-017-8598-3_5, 2014.

Koroglu, A., Ranasinghe, R., Jiménez, J. A., and Dastgheib, A.: Comparison of coastal vulnerability index applications for Barcelona Province, Ocean & coastal management, 178, 104 799, https://doi.org/10.1016/j.ocecoaman.2019.05.001, 2019.

Kourafalou, V., De Mey, P., Staneva, J., Ayoub, N., Barth, A., Chao, Y., Cirano, M., Fiechter, J., Herzfeld, M., Kurapov, A., et al.: Coastal Ocean Forecasting: science foundation and user benefits, Journal of Operational Oceanography, 8, s147–s167, https://doi.org/10.1080/1755876X.2015.1022348, 2015.

Li, Z., Shen, H., Weng, Q., Zhang, Y., Dou, P., and Zhang, L.: Cloud and cloud shadow detection for optical satellite imagery: Features, algorithms, validation, and prospects, ISPRS Journal of Photogrammetry and Remote Sensing, 188, 89–108, https://doi.org/10.1016/j.isprsjprs.2022.03.020, 2022.

Liria, P., Epelde, I., De Santiago, I., Garnier, R., Abalia, A., and Mader, J.: KOSTASystem, a coastal videometry technology: development and applications, in: 9th EuroGOOS International conference, pp. 485–491, 2021.

Mankins, J. C. et al.: Technology readiness levels, White Paper, April, 6, 1995, 1995.

https://doi.org/10.5194/egusphere-2024-3373
Preprint. Discussion started: 13 November 2024

MARLIT: Means of assessing and mitigating local coastal risks due to storm surges, https://www.azti.es/en/proyectos/marlit/, accessed: 2024-07-02, 2021.

Mateus, M., Riflet, G., Chambel, P., Fernandes, L., Fernandes, R., Juliano, M., Campuzano, F., De Pablo, H., and Neves, R.: An operational model for the West Iberian coast: products and services, Ocean Science, 8, 713–732, https://doi.org/10.5194/os-8-713-2012, 2012.

Matheen, N., Turner, I. L., Harley, M. D., Splinter, K. D., and Simmons, J. A.: How sensitive is storm erosion modelling to prior knowledge of pre-storm surf zone and nearshore bathymetry?, in: Australasian Coasts and Ports 2019 Conference: Future directions from 40 [degrees] S and beyond, Hobart, 10-13 September 2019: Future directions from 40 [degrees] S and beyond, Hobart, 10-13 September 2019, pp. 819–824, Engineers Australia Hobart, 2019.

Matheen, N., Harley, M. D., Turner, I. L., Splinter, K. D., Simmons, J. A., and Thran, M. C.: Bathymetric data requirements for operational coastal erosion forecasting using XBeach, Journal of Marine Science and Engineering, 9, 1053, https://doi.org/10.3390/jmse9101053, 2021.

Matias, A., Carrasco, A. R., Loureiro, C., Masselink, G., Andriolo, U., McCall, R., Ferreira, Ó., Plomaritis, T. A., Pacheco, A., and Guerreiro, M.: Field measurements and hydrodynamic modelling to evaluate the importance of factors controlling overwash, Coastal Engineering, 152, 103 523, https://doi.org/10.1016/j.coastaleng.2019.103523, 2019.

McCall, R., Masselink, G., Poate, T., Roelvink, J., Almeida, L., Davidson, M., and Russell, P.: Modelling storm hydrodynamics on gravel beaches with XBeach-G, Coastal Engineering, 91, 231–250, https://doi.org/10.1016/j.coastaleng.2014.06.007, 2014.

McGranahan, G., Balk, D., and Anderson, B.: The rising tide: assessing the risks of climate change and human settlements in low elevation coastal zones, Environment and urbanization, 19, 17–37, https://doi.org/10.1177/0956247807076960, 2007.

Mickey, R. C., Dalyander, P. S., McCall, R., and Passeri, D. L.: Sensitivity of storm response to antecedent topography in the XBeach model, Journal of Marine Science and Engineering, 8, 829, https://doi.org/10.3390/jmse8100829, 2020.

Nieto, M. A., Garau, B., Balle, S., Simarro, G., Zarruk, G. A., Ortiz, A., Tintoré, J., Álvarez-Ellacuría, A., Gómez-Pujol, L., and Orfila, A.: An open source, low cost video-based coastal monitoring system, Earth Surface Processes and Landforms, 35, 1712–1719, https://doi.org/10.1002/esp.2025, 2010.

Ojeda, E. and Guillén, J.: Shoreline dynamics and beach rotation of artificial embayed beaches, Marine Geology, 253, 51–62, https://doi.org/10.1016/j.margeo.2008.03.010, 2008.

Oliveira, J. N. C., Oliveira, F. S., Neves, M. G., Clavero, M., and Trigo-Teixeira, A. A.: Modeling wave overtopping on a seawall with XBeach, IH2VOF, and mase formulas, Water, 12, 2526, https://doi.org/10.3390/w12092526, 2020.

Pérez Gómez, B., Vilibić, I., Šepić, J., Međugorac, I., Ličer, M., Testut, L., Fraboul, C., Marcos, M., Abdellaoui, H., Álvarez Fanjul, E., et al.: Coastal sea level monitoring in the Mediterranean and Black seas, Ocean science, 18, 997–1053, https://doi.org/10.5194/os-18-997-2022, 2022.

Pinardi, N. and Woods, J.: Ocean forecasting: conceptual basis and applications, Springer Science & Business Media, 2002.

Quansah, J. E., Engel, B., and Rochon, G. L.: Early warning systems: a review, Journal of Terrestrial Observation, 2, 5, 2010.

Ribas, F., Ojeda, E., Price, T. D., and Guillén, J.: Assessing the suitability of video imaging for studying the dynamics of nearshore sandbars in tideless beaches, IEEE transactions on geoscience and remote sensing, 48, 2482–2497, https://doi.org/10.1109/TGRS.2009.2039576, 2010.

Roelvink, D., Reniers, A., Van Dongeren, A., De Vries, J. V. T., McCall, R., and Lescinski, J.: Modelling storm impacts on beaches, dunes and barrier islands, Coastal engineering, 56, 1133–1152, https://doi.org/10.1016/j.coastaleng.2009.08.006, 2009.

https://doi.org/10.5194/egusphere-2024-3373
Preprint. Discussion started: 13 November 2024

Roelvink, D., Reniers, A., Van Dongeren, A., Van Thiel de Vries, J., Lescinski, J., and McCall, R.: XBeach model description and manual, Unesco-IHE Institute for Water Education, Deltares and Delft University of Tecnhology. Report June, 21, 2010, 2010.

Romero-Martín, R., Caballero-Leiva, I., Llasat, M. C., Llasat-Botija, M., Rigo, T., Valdemoro, H. I., Gilabert, J., Cortès, M., and Jiménez, J. A.: Mapping cumulative compound hydrometeorological and marine-induced risks on the NW Mediterranean coast, Scientific reports, 14, 3237, https://doi.org/10.1038/s41598-024-53899-z, 2024.

Sánchez-Artús, X., Gracia Garcia, V., Espino Infantes, M., Sierra Pedrico, J. P., Pinyol Guamis, J., and Sánchez-Arcilla Conejo, A.: Present and future flooding and erosion along the NW Spanish Mediterranean Coast, Frontiers in marine science, 10, https://doi.org/10.3389/fmars.2023.1125138, 2023.

Sánchez-Artús, X., Subbiah, B., Gracia, V., Espino, M., Grifoll, M., Espanya, A., and Sánchez-Arcilla, A.: Evaluating barrier beach protection with numerical modelling. A practical case, Coastal Engineering, 191, 104 522, https://doi.org/10.1016/j.coastaleng.2024.104522, 2024.

Schiller, A., Mourre, B., Drillet, Y., and Brassington, G.: Overview of operational oceanography, New frontiers in operational oceanography, pp. 1–26, https://doi.org/10.17125/gov2018.ch01, 2018.

Schweiger, C., Koldrack, N., Kaehler, C., and Schuettrumpf, H.: Influence of nearshore bathymetry changes on the numerical modelling of dune erosion, Journal of Coastal Research, 36, 545–558, https://doi.org/10.2112/JCOASTRES-D-19-00067.1, 2020.

Scott, T., Austin, M., Masselink, G., and Russell, P.: Dynamics of rip currents associated with groynes—field measurements, modelling and implications for beach safety, Coastal Engineering, 107, 53–69, https://doi.org/10.1016/j.coastaleng.2015.09.013, 2016.

She, J., Allen, I., Buch, E., Crise, A., Johannessen, J. A., Le Traon, P.-Y., Lips, U., Nolan, G., Pinardi, N., Reißmann, J. H., et al.: Developing European operational oceanography for Blue Growth, climate change adaptation and mitigation, and ecosystem-based management, Ocean Science, 12, 953–976, https://doi.org/10.5194/os-12-953-2016, 2016.

Shen, H., Li, X., Cheng, Q., Zeng, C., Yang, G., Li, H., and Zhang, L.: Missing information reconstruction of remote sensing data: A technical review, IEEE Geoscience and Remote Sensing Magazine, 3, 61–85, https://doi.org/10.1109/MGRS.2015.2441912, 2015.

Simarro, G., Ribas, F., Álvarez, A., Guillén, J., Chic, Ò., and Orfila, A.: ULISES: An open source code for extrinsic calibrations and planview generations in coastal video monitoring systems, Journal of Coastal Research, 33, 1217–1227, 2017.

Simarro, G., Calvete, D., Luque, P., Orfila, A., and Ribas, F.: UBathy: A new approach for bathymetric inversion from video imagery, Remote Sensing, 11, 2722, https://doi.org/10.3390/rs11232722, 2019.

Simarro, G., Calvete, D., and Souto, P.: UCalib: Cameras Autocalibration on Coastal Video Monitoring Systems, Remote Sensing, 13, https://doi.org/10.3390/rs13142795, 2021.

Sotillo, M. G., Cerralbo, P., Lorente, P., Grifoll, M., Espino, M., Sanchez-Arcilla, A., and Álvarez-Fanjul, E.: Coastal ocean forecasting in Spanish ports: the SAMOA operational service, Journal of Operational Oceanography, 13, 37–54, https://doi.org/10.1080/1755876X.2019.1606765, 2020.

Stanev, E. V., Schulz-Stellenfleth, J., Staneva, J., Grayek, S., Grashorn, S., Behrens, A., Koch, W., and Pein, J.: Ocean forecasting for the German Bight: from regional to coastal scales, Ocean Science, 12, 1105–1136, https://doi.org/10.5194/os-12-1105-2016, 2016.

Taborda, R. and Silva, A.: COSMOS: A lightweight coastal video monitoring system, Computers & geosciences, 49, 248–255, https://doi.org/10.1016/j.cageo.2012.07.013, 2012.

Turki, I., Medina, R., Gonzalez, M., and Coco, G.: Natural variability of shoreline position: Observations at three pocket beaches, Marine Geology, 338, 76–89, https://doi.org/10.1016/j.margeo.2012.10.007, 2013.

Van Dongeren, A., Ciavola, P., Martinez, G., Viavattene, C., Bogaard, T., Ferreira, O., Higgins, R., and McCall, R.: Introduction to RISC-KIT: Resilience-increasing strategies for coasts, Coastal Engineering, 134, 2–9, https://doi.org/10.1016/j.coastaleng.2017.10.007, 2018.

https://doi.org/10.5194/egusphere-2024-3373
Preprint. Discussion started: 13 November 2024

Walstad, L. J. and McGillicuddy, D. J.: Data assimilation for coastal observing systems, Oceanography, 13, 47–53, https://www.jstor.org/stable/43924348, 2000.

Wilkin, J., Rosenfeld, L., Allen, A., Baltes, R., Baptista, A., He, R., Hogan, P., Kurapov, A., Mehra, A., Quintrell, J., et al.: Advancing coastal ocean modelling, analysis, and prediction for the US Integrated Ocean Observing System, Journal of Operational Oceanography, 10, 115–126, https://doi.org/10.1080/1755876X.2017.1322026, 2017.

Williams, J. J., Esteves, L. S., et al.: Guidance on setup, calibration, and validation of hydrodynamic, wave, and sediment models for shelf seas and estuaries, Advances in civil engineering, 2017, https://doi.org/10.1155/2017/5251902, 2017.

Willmott, C. J.: On the validation of models, Physical geography, 2, 184–194, https://doi.org/10.1080/02723646.1981.10642213, 1981.

Zhou, Y., Feng, X., Liu, M., and Wang, W.: Influence of beach erosion during wave action in designed artificial sandy beach using XBeach model: profiles and shoreline, Journal of Marine Science and Engineering, 11, 984, https://doi.org/10.3390/jmse11050984, 2023.